REAR FUSELAGE FLOW STUDIES ON A MODERN TRANSONIC TRANSPORT AIRCRAFT: EXPERIMENTS AND COMPUTATIONS

by

E. Coustols *, S. Prudhomme *, D. Destarac ** & A. Mignosi *

* *CERT-ONERA, Aerothermodynamics Department, Toulouse, France.*
** *ONERA, Aerodynamics Division, Chatillon, France.*

Abstract

An experimental programme has been set-up in the transonic, pressurized and self-adaptive walls T2-wind tunnel of CERT. The 1/80th scale model of a modern transonic transport aircraft has been tested for several configurations: "Fuselage alone" and "Fuselage/Horizontal stabilizer combination". The stabilizer has been set at -2° with respect to the Reference Horizontal Fuselage, while the fuselage was set at: 0° and 2.5°. Various types of measurements have been performed: oil-flow visualisations, pressure distributions, boundary layer surveys along the fuselage symmetry lines through Laser Doppler Anemometry system and wake surveys through both pressure and velocity measurements in a plane downstream of the fuselage base. Moreover, inviscid as well as viscous computations have been carried out in the conditions of the experiments; no coupling method has been used, yet. Then, it has been possible to complete a detailed analysis between computations and experiments for the afore-mentioned configurations.

Introduction

Three-dimensionnal flow separation phenomena on various parts of an aircraft receive considerable attention from designers. In the case of a commrecial transport aircraft, rear-fuselage separation, although less important than for a rear-loading cargo, is worth investigating because it is liable to be a non-negligible drag source. It should be emphasized that observations of tuft stuff during flight tests or visualisations from woollen wires in wind tunnel might not be the appropriate indicators in order to detect 3D flow separation. Generally speaking, that latter is associated with storage of fluid in the wall region and, thereby, leads to an important vortex motion which develops in the vicinity of the lower symmetry line of the fuselage and, consequently, spreads downstream of the upswept fuselage base.

This paper deals with results which are part of a long-term programme regarding rear-part of fuselage flows, initiated in mid-1990 and elaborated between S.T.P.A (Service Technique des Programmes Aéronautiques), Airbus Industrie, Aérospatiale and ONERA. The main goals of the experimental as well as numerical work were, first of all, to reach a better qualification and knowledge of the external and wall flows developing along the rear part of a fuselage of a commercial type subsonic aircraft and, secondly, to generate an important data base necessary for the validation of present and future inviscid and viscous codes, used and developed at ONERA.

Thus, those experiments consisted of "Fuselage alone" and "Fuselage/horizontal tail combination" configurations. A 1/80th scale model of a modern transonic transport aircraft has been handled, within the test section of the transonic, pressurized,and self-adaptive walls T2-wind tunnel of CERT through a fin-sting. Experiments have been performed at a stagnation pressure close to 2 bar, at ambient temperature and a free-stream Mach number of 0.82. The Reynolds number, based on the aerodynamical chord length of the model, is close to 2.5 million, which is comparable to Reynolds numbers reached for industrial wind tunnel applications, but of course less than the flight Reynolds number which is close to 50 million. Beyond the ability to provide a rather high value of the aerodynamical chord Reynolds number, that wind tunnel does permit the possibility of three-dimensional Laser Doppler Anemometry measurements either on the model itself or in its wake.

For several configurations, numerous types of measurements have been performed: oil-flow visualisations, pressure distributions (the model has been equipped with almost 140 pressure taps), boundary layer surveys along the upper and lower symmetry lines using LDA system and wake sur-

veys through both pressure and velocity measurements in a plane located at approximately two diameters downstream of the fuselage base.

Moreover, inviscid as well as viscous computations have been carried out in the conditions of the experiments; no coupling method has been developed, yet. The external flow has been computed from a surface panel method, while the local three-dimensional boundary layer equations have been solved using a characteristic method. Then, it has been possible to complete a detailed analysis between computations and experiments for the tested configurations. The typical features of that experimental as well as numerical work are developed in the present paper.

It should be noted that this should be the first set of experiments (at least, to our knowledge) dealing with the effect of the horizontal stabilizer on the wall flow in the rear part of the fuselage.

Wind tunnel conditions

Experimental Set-Up - Model

The T2 wind tunnel at CERT/DERAT

That tunnel is an induction driven facility, the circuit of which is closed. It is a pressurized, transonic, cryogenic and self-adaptive wall wind tunnel. Each run is 30 up to 120 second long. The flow is driven by an injection of dry air at ambient temperature cooled by another injection of liquid nitrogen for cryogenic conditions.[1] The standard operating range is: M_∞: 0.6-0.9, Pi_∞: 1.3-3.0 bar and Ti_∞: 120-300 K.

The test section is 0.39 m wide, 0.37 m high and 1.42 m long. The use of top and bottom flexible walls allows to avoid transonic blockage and minimize wall interference effects; those walls can be controlled by either a two-dimensional or a three-dimensional strategy.[2,3] They are moved by 16 hydraulic jacks, allowing 0.2 mm step-by-step displacement up to a maximum variation of 25 mm, acting upon invar steel sheets. That adaptive wall capability allows to consider rather large models and provides very accurate results.

The interest of considering that wind tunnel, for rear fuselage flow applications, is that, besides the ability to provide high values of the Reynolds number, it has been equipped for three to four years now with a three-dimensional LDA system.[4,5] Thus, detailed secondary fields, the knowledge of which is crucial for vortex flows, could be recorded.

Model

The model of a modern transonic transport aircraft has been designed and manufactured at IMF Lille; its scale is 1:80. It consists of the fuselage and its horizontal stabilizer. The length of the fuselage and the diameter of the cylindric part are 0.733 m and 0.070 m, respectively. Compared to the real plane, the horizontal tail/fuselage gap is missing, and the horizontal stabilizer shield is not represented. However, experiments performed rather recently showed up that these small modifications were not prejudiciable to the main characteristics of the rear-fuselage flow, although the absence of gap would impede possible connection between the lower and upper parts of the fuselage.

Experimental set-up

The model is handled in the test section using a fin-sting (figure 1). Because of structural problems, the model fin is geometrically changed from the scaled aircraft fin, but the chord at the fuselage/fin junction as well as the sweep angle of the leading edge are correct.

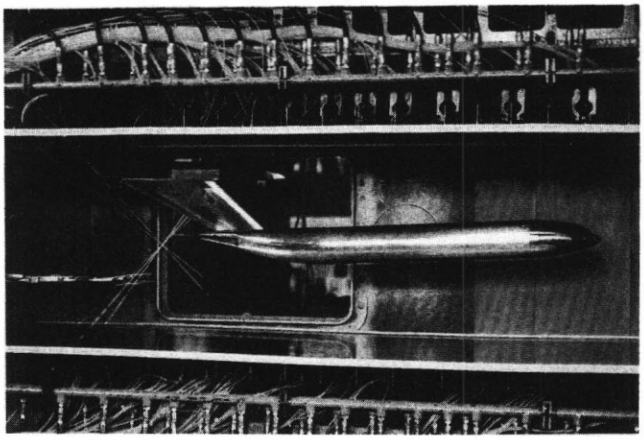

Figure 1: View of the model in the T2 test section, handled using a fin-sting.

The sting itself induced interferences along the centre-line of the test section, in the field where the upswept rear-fuselage will be set, later on. The use of the flexible upper and lower walls of the test section allows to balance this interference. So, the wall and the sting interferences are cancelled on the fuselage axis. Velocity measurements, performed during that campaign, allowed to verify that the residual disturbances were rather small.[3]

Instrumentation

The fuselage of the model was equipped with 139 static pressure taps; 115 were located on half-side of the rear part of the fuselage along the last last 32% of the fuselage length. For a couple of streamwise sections, taps located in the same horizontal plane allowed to verify that the model is not set at some angle of yaw. The rather important number of pressure measurements in that

downstream part of the fuselage made it possible to define, precisely enough, both the streamwise evolution of the pressure along the symmetry lines, and the azimuthal distribution of the pressure; thus, that would help when looking at the influence of the tailplane on the external flow.

For wake surveys, a pressure rake, the width of which was 125 mm, was defined. It consisted of 2 decks: the upper one is made of 8 total pressure probes and the lower one of 6 static ones. Besides the two extreme total pressure probes, all the probes are set at equal distance: 25mm and 15mm for the static and total probes, respectively. Calibration of this rake was performed, without the model, at the beginning of the campaign; but, because of its obstruction, some residual corrections were applied to the static values, using LDA system.

The three-dimensional LDA system was used for boundary layer and wake surveys. The diameter of the measuring volume, tightly related to the intersection of the three coloured beams as well as their waists, was close to 130μm for any configuration (forward or backward scattering). Regarding nearer wall approaches, using forward scattering (tangential approach, for the symmetry lines of the model) one could go as close as 0.3-0.4 mm to the wall; however, considering backward scattering (normal approach, mid-lateral line on the fuselage), the shortest distance to the wall was 3.0 mm.

Test conditions

Tests were carried out at a stagnation pressure of 1.95 bar, at ambient temperature (300 K), for a free-stream Mach number of 0.82. That leads to a chord Reynolds number, R_c, based on the aerodynamical chord length of the model (0.091 m), close to 2.5 million.

Transition was tripped on the fuselage (carborundum band, average height: 45μm at 12 mm from the nose) and on the lower and upper sides of the horizontal tail (carborundum band, average height: 35μm at 5% of the local chord length). Natural transition occurred on the vertical fin, yet.

If α denotes the angle of attack of the fuselage and α_e corresponds to the setting of the horizontal stabilizer with respect to the Reference Horizontal Fuselage line, several configurations were tested:
a) α=0° (without the horizontal stabilizer);
b) α=2.5° (without the horizontal stabilizer);
c) α=0° - α_e=-2° (with the horizontal stabilizer);
d) α=2.5° - α_e=-2° (with the horizontal stabilizer).

Measurements

In order to reproduce as correctly as possible the external flow around the model, the adaptation of the flexible walls of the test section had to be derived, according to methods developed at DERAT.[2,3] For each test configuration, the final geometry of the upper and lower flexible walls was obtained by adding to the shape, already adapted onto the presence of the model and lateral boundary layers, the displacements necessary to counteract the perturbations due to the sting itself; that deformation is added using linearity assumption.

Once the adaptation process was carried out, the following measurements were done:
- oil-flow visualisations on the rear part of the fuselage and on the horizontal and vertical stabilizers.
- streamwise pressure distributions on the rear part of the fuselage and along the upper and lower symmetry lines; azimuthal evolution of the pressure for given streamwise sections.
- boundary layer surveys at several streamwise abscissae along the symmetry lines of the model using forward scattering.
- wake surveys through both velocity and pressure measurements, in one plane located at approximately two diameters downstream of the fuselage base. In fact, regarding pressure measurements, a complete plane was investigated, while one half of the wake was only looked at for velocity purpose.

It should be reasonable to believe that the combination of such measurements be a good data source useful for physical understanding of the flow effects on the rear part of the fuselage.

Inviscid and viscous flow computations

Following on inviscid calculations performed for the conditions of the tested configurations, boundary layer codes were run. Then, comparisons with experimental results could be investigated.

Potential flow computations

The potential flow was computed by the panel method used at ONERA but developed at Aérospatiale.[6] This is a source-vortex method. The surface of the aircraft is represented by quadrilateral panels, called skin panels, bearing sources of constant strength. Lifting surfaces enclose so called skeleton panels, which support vortices of strength varying linearly in the streamwise direction, and piecewise constant in the spanwise direction. Wakes are modelled by vortices of strength equal to that of the trailing edge squeleton panels. Flow tangency is ensured on the skin panels, and Kutta conditions are applied at the trailing edges. Compressibility is modelled according to the Prandtl-Glauert approximation.

For half a geometry of fuselage, numbers of skin panels are 4320 in the fuselage-horizontal stabilizer-sting configuration, and 3440 in the case without horizontal stabilizer. Appropriate symmetry conditions complete the configurations. The grids were provided by Aérospatiale; they include the mesh of the fin-sting. Aerodynamic conditions are: M_∞=0.82 and α=0° or α=2.5°.

Drawings of computed isobar contours will be discussed in the following paragraphs and compared to experimental distributions.

Boundary layer computations

The 3D boundary layer equations were solved using a characteristic method; the code has been developed for these last years, at CERT, by Houdeville and co-workers.[7-9] The the momentum equations are discretized along the local streamlines within the viscous layer. This method has revealed its efficiency for applications such as prolate spheroid[8] or missiles.[9] Furthermore, one of the originalities of this method is that computations can be handled for non regular meshes.

The numerical scheme integrates Prandtl equations along the local streamlines, which are subcharacteristic lines. Thus, integration could proceed always in the same direction, whatever the crossflow direction is. The discretization of the equations is done in the plane tangent to the surface of the fuselage, using a coordinate system which respects the metric properties of the fuselage to express the derivatives of the velocity. This has been done by orthogonally projecting the body fitted coordinate system and the velocity field in the tangent plane at the considered points.[8,9] Then, the integration of the boundary layer equations could be performed using their local cartesian form, even in areas where the mesh is not regular, which is the case in the vicinity of the fuselage/tail footprints, for instance.

In such a cartesian frame, the boundary layer equations read:

$$\frac{\partial \rho u}{\partial x} + \frac{\partial \rho v}{\partial y} + \frac{\partial \rho w}{\partial z} = 0$$

$$u\frac{\partial u}{\partial x} + v\frac{\partial u}{\partial y} + w\frac{\partial u}{\partial z} = -\frac{1}{\rho}\frac{\partial p}{\partial x} + \frac{1}{\rho}\frac{\partial \tau_x}{\partial y}$$

$$0 = -\frac{1}{\rho}\frac{\partial p}{\partial y}$$

$$u\frac{\partial w}{\partial x} + v\frac{\partial w}{\partial y} + w\frac{\partial w}{\partial z} = -\frac{1}{\rho}\frac{\partial p}{\partial z} + \frac{1}{\rho}\frac{\partial \tau_z}{\partial y}$$

$$u\frac{\partial h_i}{\partial x} + v\frac{\partial h_i}{\partial y} + w\frac{\partial h_i}{\partial z} = -\frac{1}{\rho}\frac{\partial}{\partial y}(u\,\tau_x + w\,\tau_z - \phi)$$

with:

$$\tau_x = \mu\frac{\partial u}{\partial y} - \overline{(\rho v')\,u'}$$

$$\tau_z = \mu\frac{\partial w}{\partial y} - \overline{(\rho v')\,w'}$$

$$\phi = -\lambda\frac{\partial T}{\partial y} + \overline{(\rho v')\,h'}$$

and

$$h_i = h + \frac{u^2 + v^2}{2}$$

In those equations, μ, ρ and λ denote dynamical viscosity, density and thermal conductibility of the fluid, whereas h and h_i are the static and stagnation enthalpy, respectively. The subscripts l and t refer to the laminar and turbulent cases. The unknowns of this system are the three components of the velocity as well as h_i, the knowledge of which allows to calculate the local temperature.

The solution of the preceding equations needs boundary conditions both at the wall (impermeable wall) and at the edge of the boundary layer (data given from the solution of the inviscid flow equations). Initial laminar conditions are deduced from similarity solutions (stagnation point in 3D flows). Then, transition was fixed according to the experimental location on the fuselage.

Along the lower symmetry line of the rear part of the fuselage, the boundary layer grows rapidly, and its thickness is not negligible compared to the transverse curvature of the fuselage cross-sections. Then, a corrective term has been introduced in the continuity equation, affecting mainly the derivative of the transverse component of the velocity.

The computation of a 3D turbulent boundary layer requires the adjunction of a turbulence model to express the components of the Reynolds shear stresses, $-\overline{(\rho v')u'}$ and $-\overline{(\rho v')w'}$. Among others, results given by a mixing length model and a two-layer model will be presented.

Mixing length model

This is the simplest model, based upon the assumption that the shear stress vector has the same direction as the velocity gradient vector:

$$-\overline{(\rho v')\,u'} = \rho F^2 l^2 \left(\sqrt{(\frac{\partial u}{\partial y})^2 + (\frac{\partial w}{\partial y})^2}\right)\frac{\partial u}{\partial y}$$

$$-\overline{(\rho v')\,w'} = \rho F^2 l^2 \left(\sqrt{(\frac{\partial u}{\partial y})^2 + (\frac{\partial w}{\partial y})^2}\right)\frac{\partial w}{\partial y}$$

where the mixing length, l, is defined by:

$$\frac{l}{\delta} = 0,085\,\tanh(\frac{\chi}{0,085}\frac{y}{\delta}) \quad \text{with} \quad \chi = 0.41$$

Near the wall, that expression needs to be corrected in order to take into account the wall and viscosity effects upon turbulence. The original damping function, suggested by Van Driest and improved by Cebeci and Smith[10] to take into account streamwise pressure gradients, has been considered.

Two-layer model

• In the outer region, the standard k-ϵ model, the original version of which was proposed by Jones and Launder,[11] has been used. The transport equations for the turbulent kinetic energy and the dissipation rate are recalled:

$$\rho\, u\, \frac{\partial k}{\partial x} + \rho\, v\, \frac{\partial k}{\partial y} + \rho\, w\, \frac{\partial k}{\partial x} = P_k - \rho\, \epsilon + \frac{\partial}{\partial y}\left[(\mu + \frac{\mu_t}{\sigma_k})\, \frac{\partial k}{\partial y}\right]$$

and

$$\rho\, u\, \frac{\partial \epsilon}{\partial x} + \rho\, v\, \frac{\partial \epsilon}{\partial y} + \rho\, w\, \frac{\partial \epsilon}{\partial x} = C_{\epsilon 1}\, \frac{\epsilon}{k}\, P_k - C_{\epsilon 2}\, \rho\, \frac{\epsilon^2}{k} + \frac{\partial}{\partial y}\left[(\mu + \frac{\mu_t}{\sigma_\epsilon})\, \frac{\partial \epsilon}{\partial y}\right]$$

In those equations, the production term is given from:

$$P_k = -\overline{(\rho v')u'}\, \frac{\partial u}{\partial y} - \overline{(\rho v')w'}\, \frac{\partial w}{\partial y} = \mu_t \left[(\frac{\partial u}{\partial y})^2 + (\frac{\partial w}{\partial y})^2\right]$$

and the turbulent viscosity is deduced from the turbulent kinetic energy and its dissipation rate:

$$\mu_t = \rho\, C_\mu\, f_\mu\, \frac{k^2}{\epsilon}$$

with

$$f_\mu = \exp\left(\frac{-3.4}{(1 + \frac{R_t}{50})^2}\right) \qquad R_t = \frac{k^2}{\nu\, \epsilon}$$

The values of the different constants are:

$$C_\mu = 0.09\ ;\ C_{\epsilon 1} = 1.44\ ;\ C_{\epsilon 2} = 1.92$$

$$\sigma_\epsilon = 1.3\ ;\ \sigma_k = 1.0$$

• In the near wall region, only the k-equation is solved. That model was originated, first of all, by Bradshaw for the external part of a turbulent boundary layer. Later on, Wolfshein[12] and Norris and Reynolds[13] made some improvements to handle viscous sub-layer. The system is closed by considering the following relationships for the dissipation rate and the eddy viscosity:

$$\epsilon = \frac{k^{3/2}}{L_\epsilon} \qquad \mu_t = \rho\, C_\mu\, L_\mu\, \sqrt{k}$$

where:

$$L_\epsilon = \frac{L_y}{1 + \frac{5.3}{Re_y}}$$

$$L_\mu = L_y \left(1 - exp\,(-\frac{Re_y}{50.5})\right)$$

$$L_y = \chi\, C_\mu^{-\frac{3}{4}}\, y \qquad Re_y = \frac{\sqrt{k}\, y}{\nu}$$

• The matching between the modelling in the outer and inner wall region is performed at a point where y^+ ($=y\cdot\sqrt{\frac{\tau_w}{\rho_w}}/\nu_w$) is close to 75.

Results and discussions

In this paragraph, comparisons between experimental and computational results are presented for various aerodynamic configurations. For boundary layer data, emphasise will be often given to the configuration: α=0°, α_e=-2°. On the other hand, in the wake of the model, results for both incidences of the fuselage are discussed.

Pressure field

The rather great number of pressure taps on the rear part of the fuselage has allowed to get a nice overview of the pressure field in that region. Plots of the contours of constant pressure coefficient are given on figure 2, for the configurations without and with the horizontal stabilizer.

Flow is almost uniform on the cylindric part of the model. Regarding the rear part of the fuselage, the flow is decelerating just ahead of the leading edge of the fin/fuselage junction. Downstream of that area, the flow is then accelerating up to the maximum cross-section of the fin footprint.

One could notice an increase in the external velocity field in the neighbourhood of the flat surface, which allows rotation of the horizontal tail; that surface is restricted to: 0.641m≤X≤0.716m. When comparing to the computed external pressure field, there is a rather good agreement, whatever configuration is concerned, although the number of pressure taps might not be enough on a given section to complete a very accurate comparison. However, important discrepancies exist in the last rear part and in the vicinity of the lower symmetry line. Along that line the experimental

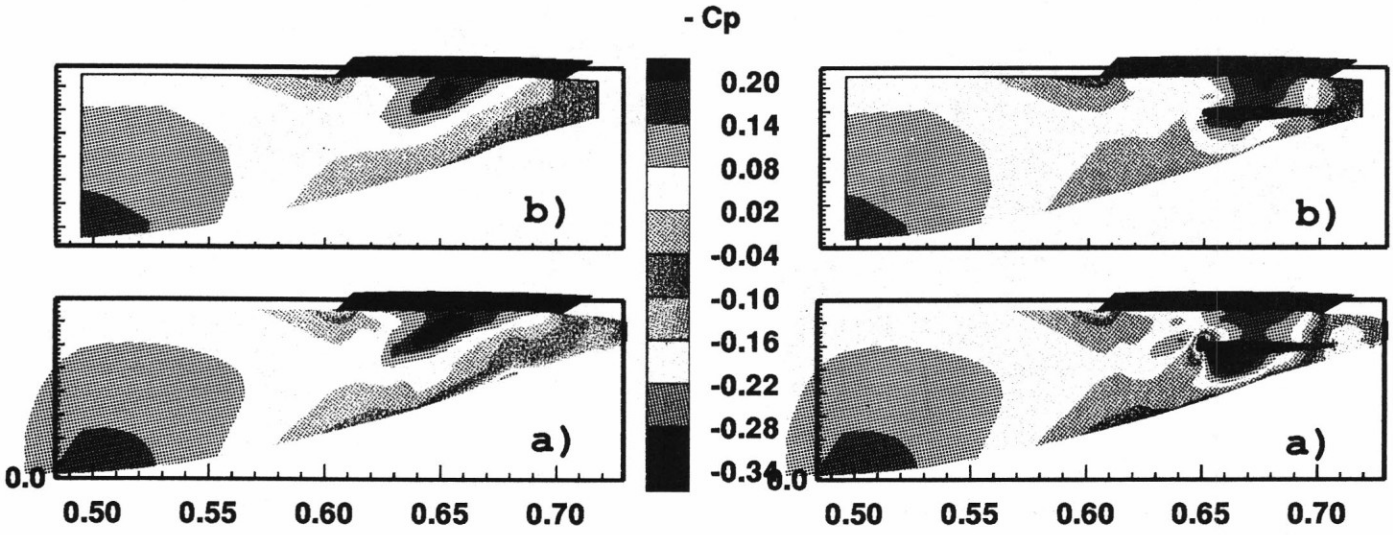

Figure 2: Coloured contours of constant pressure coefficient on the rear fuselage for α=0° - Left-hand side: without the horizontal stabilizer - Right-hand side: with the horizontal stabilizer - (a) Inviscid calculations - b) Experiments).

pressure level as well as the streamwise pressure gradient differ from the computed ones (figure 3).

In this area, the thickening of the boundary layer is rather important and, consequently, the absence of coupling between inviscid and viscous calculations could partly explain the recorded differences. The measured pressure gradient is almost equal to zero; that would suggest that the mentioned rapid growth balanced the decrease of the fuselage cross-section.

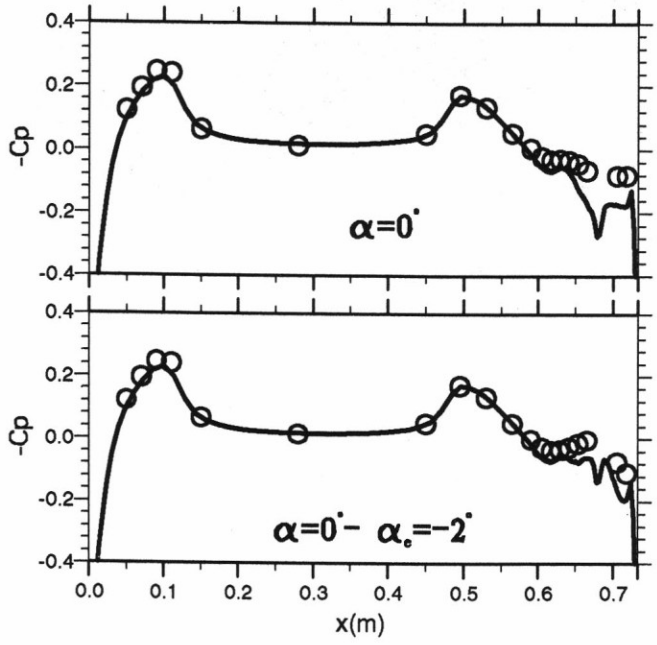

Figure 3: Streamwise pressure gradient along the lower symmetry line. — Inviscid calculations ; o Experiments - Upper part: without the horizontal stabilizer α=0° - Lower part: with the horizontal stabilizer α=0° - α_e=-2°.

When the horizontal tailplane is set at -2° with respect to the Reference Horizontal Fuselage, the pressure distribution is locally altered (figure 2). The flow is accelerated in the upper part of the fuselage, ahead of the leading edge of the horizontal tail, as well as below the lower side of it. These observations are more pronounced at α=2.5° than α=0°. It should be pointed out that the lift coefficient of the horizontal stabilizer is strongly negative for α=0°, but slightly positive for α=2.5°. The "negative" peak on the computed Cp distribution, around X=0.68 m (figure 3), corresponds to a geometrical inflexion in the lower symmetry line.

Wall pattern

Oil flow visualisations have been performed on different parts of the model. It is reasonable to believe that such visualisations would be a nice indicator of the wall-flow pattern and allow comparisons with the computed wall streamlines.

For the configuration without horizontal tail, visualisations showed some deviation of the wall flow downstream of the cylindrical part of the fuselage, and some weak accumulation of wall flow, concentrated along the upper and lower edges of the flat surface, which allows rotation of the horizontal tail (figure 4). Consequently, it is downstream of the upsweep that is initiated the vortex roll-up; its footprint will be clearly evidenced later on in the wake of the model.

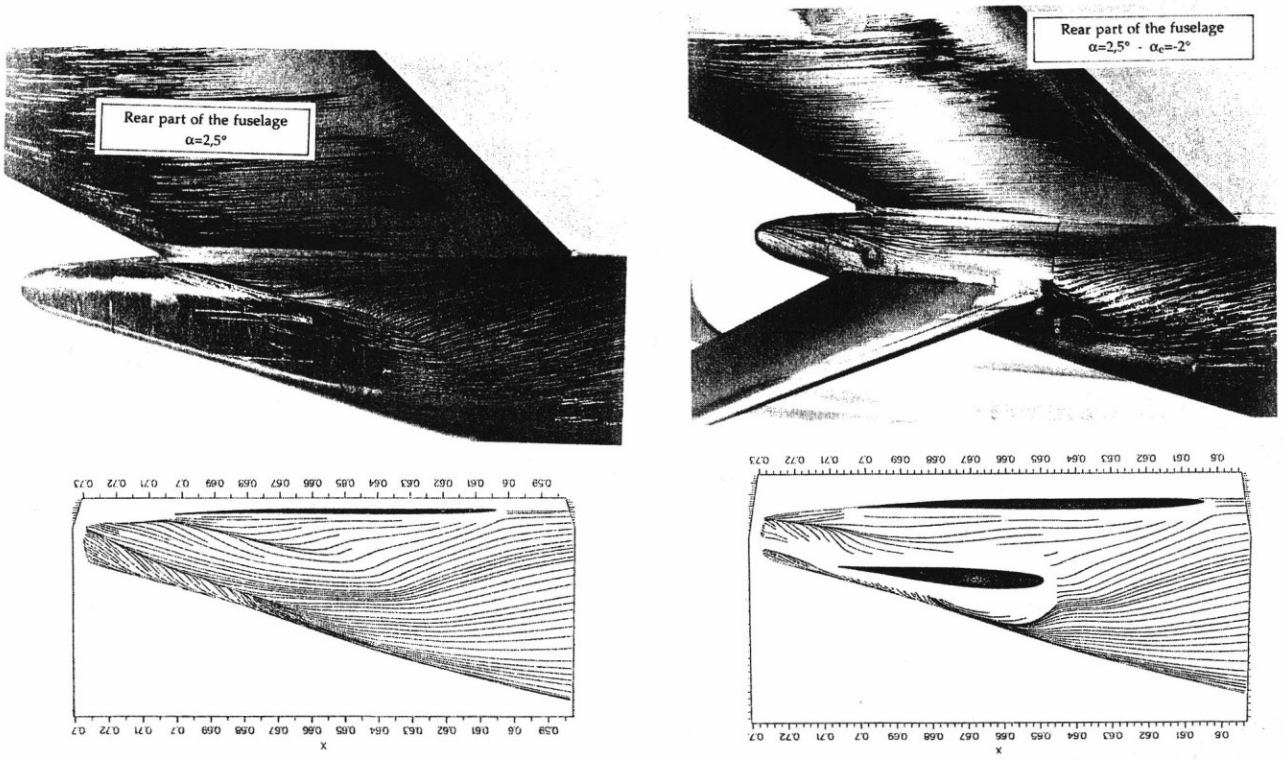

Figure 4: Drawings of parietal streamlines on the rear part of fuselage. Comparisons experiments/computations. Left-hand side: α=2.5° (without the horizontal stabilizer) - Right-hand side: α=2.5° - α_e=-2° (with the horizontal stabilizer).

The computed wall flow pattern is identical, whatever turbulence model is concerned.

Calculations revealed that tremendous wall deviations (β_0) were associated to the azimutal locations of those wall streamlines accumulations; indeed, values of β_0 close to 50° were recorded in the lower rear part of the fuselage. The agreement with the picture resulting from the oil-flow visualisation is rather good. Nevertheless, it is very hard to confirm the computed wall motion in the vicinity of the lower symmetry line.

When the fuselage is equipped with the horizontal stabilizer, one could still observe a convergence of wall streamlines along the upper part of the fuselage (figure 4). In this area, the pressure gradient is stronger than for the configuration without the horizontal tail, justifying that this convergence of wall streamline occured further downstream. Such a motion seems to be correctely captured by the boundary layer code.

Regarding the lower part of the fuselage, the convergence of wall streamlines is spectacular, inducing an upward motion of wall flow from the symmetry line towards the maximum cross-section of the horizontal stabilizer (figure 5). The existence of intense cross-flow pressure gradients, be-

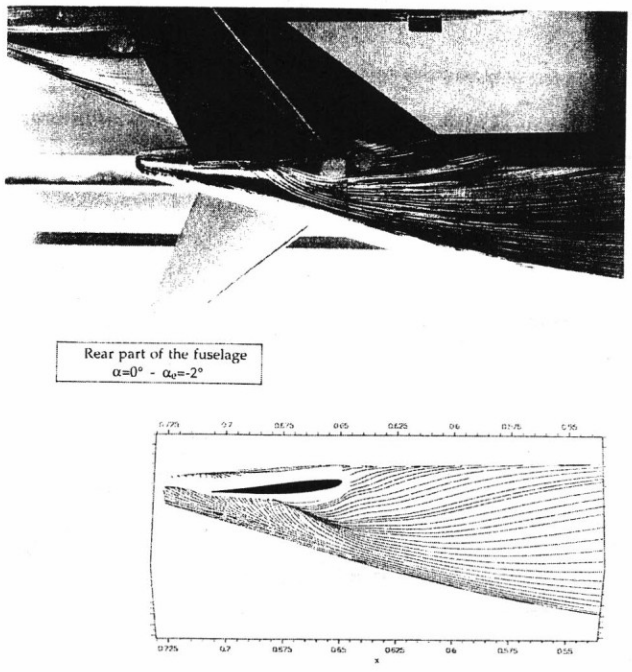

Figure 5: Drawings of parietal streamlines on the rear part of fuselage. α=0° - α_e=-2° (with the horizontal stabilizer) - Comparisons experiments/computations.

low the upstream part of the stabilizer, could induce a suction effect and, consequently, confirm such a motion. Of course, such a wall pattern gives rise to a vortex motion, the vertical development of which is restricted because of the presence of the tailplane. One could, hopefully, notice a dark triangle area on the lower side of the horizontal stabilizer, close to the junction with the fuselage, where oil could gather because of low friction.

Computations reproduce rather correctly the recorded behaviours, although the curling motion might be weaker in the computations. Of course, in the vicinity of the tail, the boundary layer code stopped because of the intensity of both the streamwise and azimutal pressure gradients. It could be noteworthy to mention that, for azimutal locations as far as 50° away from the lower symmetry line, β_0 is comparable to, and even less than, the one recorded for the same value of α, but without the horizontal tail. That means that the boundary layer development in this area is dictated by the fuselage geometry (upsweep, more especially) and not the presence of the horizontal tail.

Boundary layer surveys

The 3D-LDA measurement system allows to perform several boundary layer surveys for given streamwise locations on the upper and lower symmetry lines. Velocity profiles are plotted in a coordinate system associated with the boundary layer: Y is the direction normal to the wall, X and Z are in the plane, tangent to the wall, with X in the direction of the free-stream velocity.

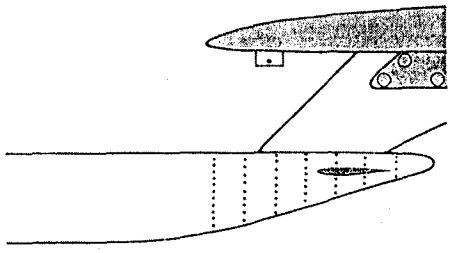

Figure 6: Locations of boundary layer surveys.

For these measurements, the LDA system is operating in the forward scatter mode in order to obtain better accuracy, measurement quickness and access to the flow in the near wall region. Along the lower and upper symmetry lines, the velocity component in the Z-direction, does not exceed 2-3 ms^{-1}, while the external free-stream velocity is close to 260 ms^{-1}. Thus, that allows to verify, not only the perfect symmetry of the flow but also that the measurement volume is correctly located, along both symmetry lines.

A couple of surveys have been performed on the upper symmetry line, in front of the fin. On the lower symmetry line, seven measurement stations were defined between X=0.565 m and X=0.718 m, i.e. approximately 77% and 98% of the fuselage length (figure 6). Results discussed below correspond to the α=0° - α_e=-2° configuration.

• Mean quantities

For the most upstream section, the mean velocity profiles are plotted on figure 7, for the upper and lower symmetry lines. The considered turbulence models do not have any effect on the mean streamwise and normal to the wall velocity components. The agreement between computations and measurements is rather good, above all on the V-component which is rather small, since its modulus is less than 0.1 U_e.

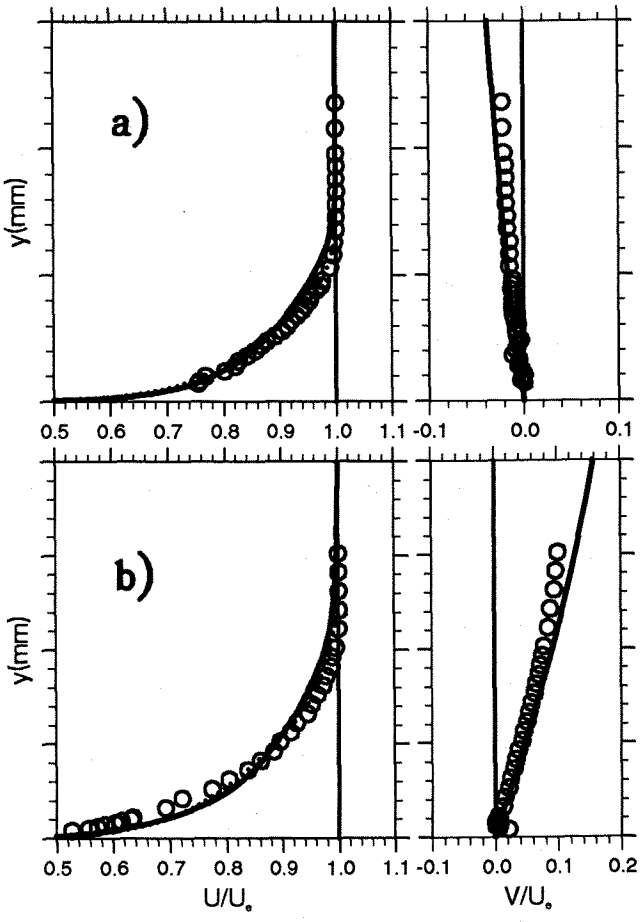

Figure 7: Streamwise and normal to the wall velocity components at X=0.565 m along a) Upper symmetry line b) Lower symmetry line - ... Mixing length model; — Two-layer model; o Experiments: α=0° - α_e=-2° (with the horizontal stabilizer).

Following on the development of the boundary layer along the lower symmetry line, the two components of the velocity are plotted on figure 8 for X=0.617 m and 0.665 m, respectively.

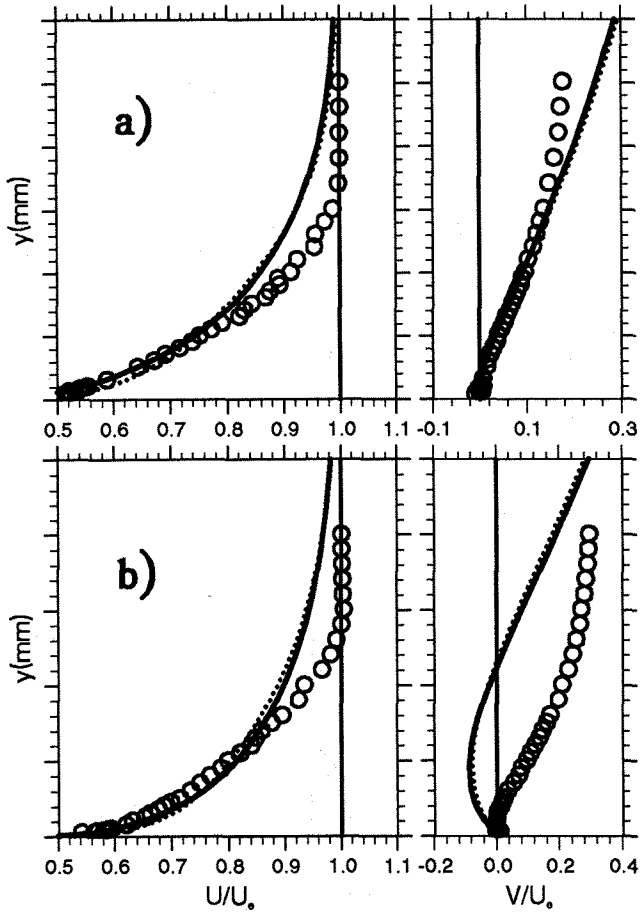

Figure 8: Streamwise and normal to the wall velocity components along the lower symmetry line at a) X=0.617 m b) X=0.665 m - ... Mixing length model; — Two-layer model; o Experiments: α=0° - α_e=-2° (with the horizontal stabilizer).

The thickening of the boundary layer is rather important at this angle of attack, approximately 15% greater than at α=2.5°. Calculation overpredicts the boundary layer growth and, consequently, V_e appears to be greater than the experimental value. In the outer edge of the boundary layer, the experimental value of $\partial V/\partial y$ is equal to zero, since the pressure is roughly constant or weakly increasing. On the other hand, the computed value of $(\partial V/\partial y)_{y=\delta}$ varies as the pressure gradient, since it is equal to - $\partial U_e/\partial x$ (continuity equation).

Even though transverse curvature has been taken into account in the continuity equation, the increase of boundary layer thickness is large; in fact, for X> 0.65 m, δ is even greater than the largest dimension of the fuselage cross-section. One can be very suspicious regarding the reliability of boundary layer assumptions in such areas. Downstream X=0.617 m, the shape of the computed U-profile is very different from the experimental one. The recorded variations on both pressure level and pressure gradient are not strong enough for explaining such differences on the two components of the mean velocity profiles. Indeed, the used numerical codes cannot reproduce a possible interaction between the boundary layer development along the lower symmetry line and the vortex motion which spreads downstream of the cylindric part of the fuselage.

- Fluctuating quantities

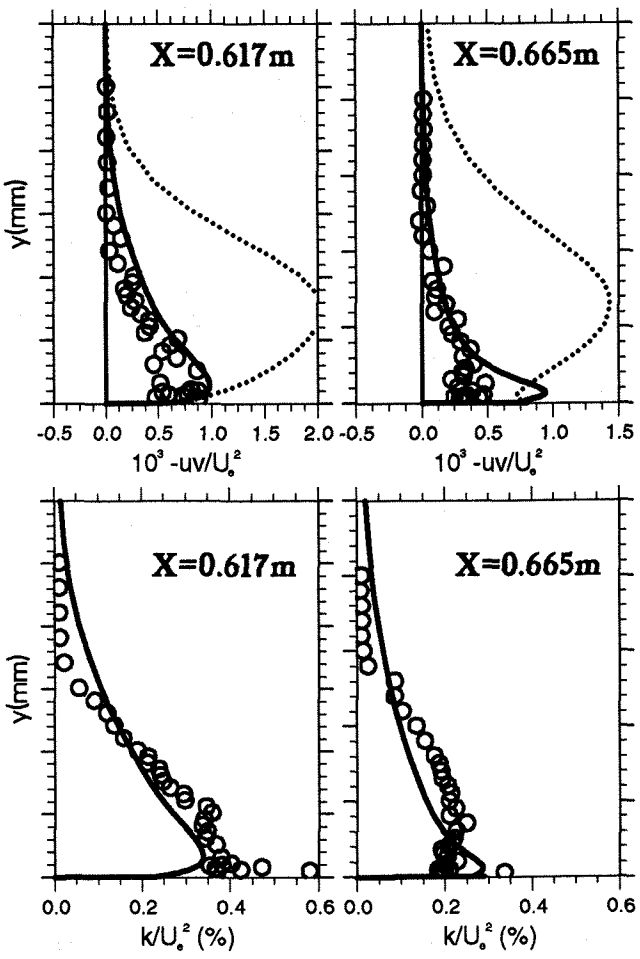

Figure 9: Shear stress and kinetic energy profiles along the lower symmetry line at X=0.617 m and X=0.665 m - ... Mixing length model; — Two-layer model; o Experiments: α=0° - α_e=-2° (with the horizontal stabilizer).

The shear stress and kinetic energy profiles are plotted on figure 9 for X=0.617 m and 0.665 m.

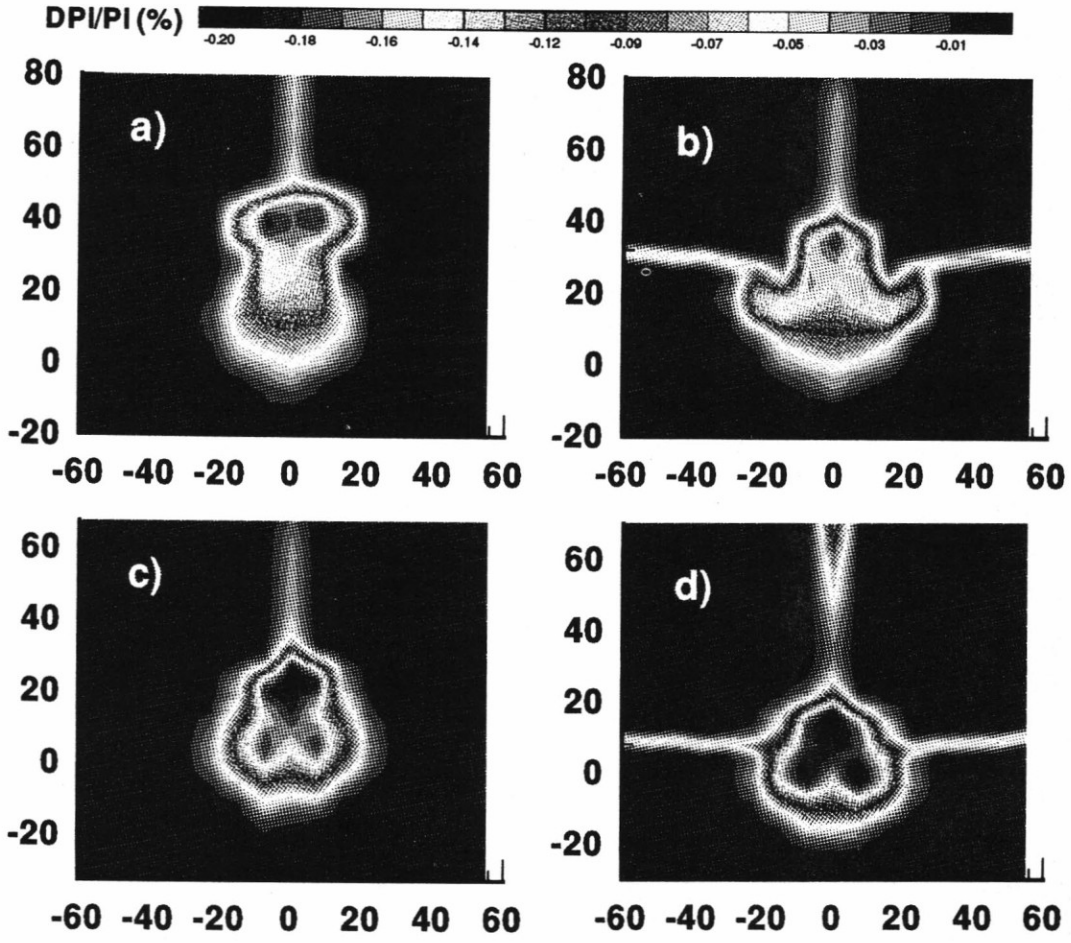

Figure 10: Contours of constant stagnation pressure loss in the wake at two diameters downstream of the fuselage base. a) α=0° (without horizontal stabilizer) - b) α=0° - α_e=-2° (with horizontal stabilizer) - c) α=2.5° (without horizontal stabilizer) - d) α=2.5° - α_e=-2° (with horizontal stabilizer).

Contrary to the mean velocity profiles, the turbulence model has some effect; the two-layer model provides much better results. For X=0.665 m, the estimate of shear stress in the near wall region is not satisfactory; the computed profile exhibits a rather important peak, due to the flow acceleration, while the measured shear stresses are lower. In this area where 3D effects prevail, one could question the assumption that the shear stress vector has the same direction as the mean velocity gradient vector.

The computed k-profile, when applying the two-layer model, is plotted versus y, although there has been no attempt to estimate turbulent kinetic energy, when using a mixing length model. The experimental k values are deduced from:

$$k = \frac{\overline{u'^2} + \overline{v'^2} + \overline{w'^2}}{2}$$

Close to the wall, the turbulence level ($\sqrt{k}/U_e$) is relatively high and, then, decreases at further downstream sections; moving away from the wall, the turbulence intensity is constant over almost 30% to 40% of δ.

Wake surveys

First of all, it is noteworthy to emphasize the good consistency of pressure and velocity measurements, from wake surveys performed in a plane located at about two diameters downstream of the fuselage base; that plane is orthogonal to the direction of the free-stream. The secondary velocity field is obtained from about 600 3D-LDA measurement points (forward scattering mode), distributed all over a half-wake plane.

• Pressure measurements

The variations of the stagnation pressure in that plane are given in figure 10; the following comments can be made:

- the symmetry of measurements is rather good, especially when the horizontal tailplane is set.
- the wakes from the vertical and horizontal stabilizers are clearly evidenced; the maximum pres-

sure loss downstream of the horizontal plane is roughly constant and equal to 5%.
- for the "Fuselage alone" configuration, three defect velocity pockets are recorded in the fuselage wake. The highest one comes both from the fuselage base and the convergence of wall flow along the upper edge of the flat surface which allows rotation of the horizontal tail; the two lowest ones, symmetrical with respect to the wake axis, seem to be initiated from the vortex roll-up, the birth of which is tightly related to the upsweep, spreading along the lower part of the fuselage. A maximum deficit of 16-17% is recorded. The shape of the wake depends upon α; its size is smaller than the maximum cross-section of the fuselage.
- when the horizontal tailplane is set, the levels of defect velocity pockets are re-distributed within the wake. The effect of the tail is more pronounced at α=0°, where a sharp peak in the isobars plot can be observed; this has to be related to strong downwards negative velocities, as it will be discussed later on.

• Velocity measurements

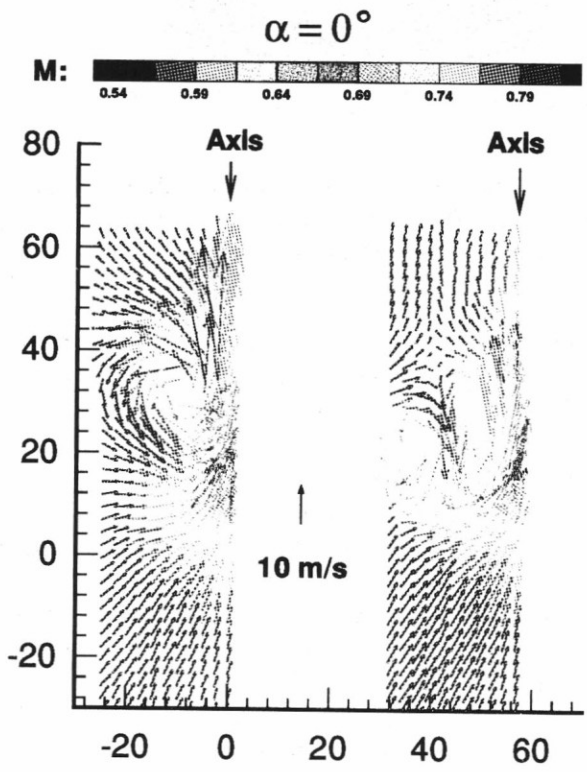

Figure 11: Secondary velocity field at two diameters downstream of the fuselage base, for α=0° - Left-hand side: without the horizontal stabilizer - Right-hand side: with the horizontal stabilizer.

The secondary velocity field is plotted in figures 11 and 12, for α=0° and 2.5°, respectively. The colour of the small arrows is graduated with respect to the intensity of the local Mach number. There is a good consistency between pressure and velocity measurements: important vertical velocities are recorded in areas where vortex activity is intense, where Mach numbers are small, i.e where pressure loss is maximum. Indeed, that would suggest in the same time that pressure loss could be identified as vortex flow.

Those measurements reveal the existence of a single vortex in each half-wake plane, for the "Fuselage alone" configuration. Its location is higher and its intensity stronger at α=0° than at 2.5°. Along the wake centre-line, rather large vertical velocities (almost 50 ms^{-1} at α=0°) were recorded.

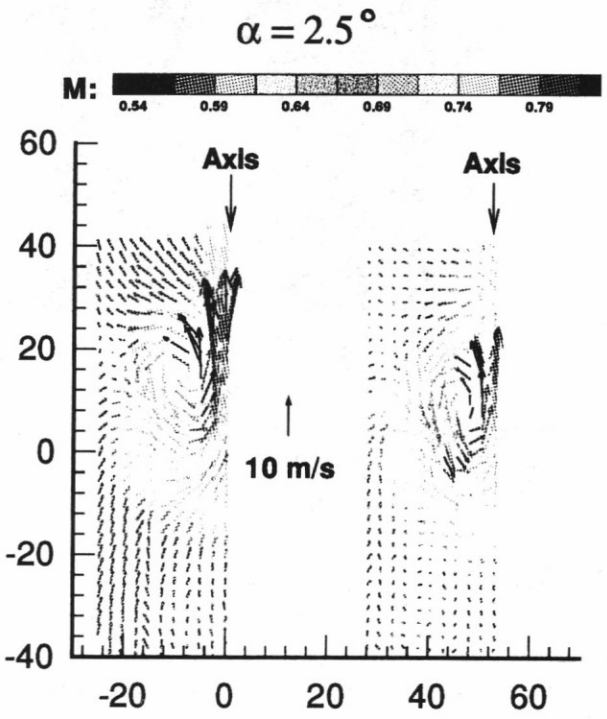

Figure 12: Secondary velocity field at two diameters downstream of the fuselage base, for α=2.5° - Left-hand side: without the horizontal stabilizer - Right-hand side: with the horizontal stabilizer.

The horizontal tail generates a second contra-rotating vortex in each half-plane; its centre is located below the main vortex one, further away from the wake axis (figures 11 and 12). When the fuselage is at α=2.5°, an extra "small" vortex could be identified just above the tailplane / fuselage junction.

Furthermore, at α=0°, the overall fuselage wake is moving slightly downwards, according to the negative lift coefficient of the horizontal tailplane; on the other hand, this displacement effect is neg-

ligible at α=2.5°. For α=0°, the interaction of the two vortices creates rather large negative velocity components, justifying the afore-mentioned sharp shape on the contours of constant stagnation pressure (figure 10 d))

Knowing the two secondary velocities, it has been possible to compute the streamwise component of the rotational (Ω_x=∂W/∂Y - ∂V/∂Z) and, consequently, not only to define rather precisely the centre of each vortex system, but also to integrate Ω_x all over each half-wake plane. By doing so, one ends up for the configuration with the horizontal tail with an overall vorticity weaker than for the case without horizontal tail. Generally speaking, the intensity of the main strongest vortex is weakened, whatever the angle of attack of the fuselage is.

• Variations of drag coefficient

From wake surveys performed through both velocity and pressure measurements, the total drag coefficient of the model could be estimated. Indeed, pressure measurements are inadequate since they provide only the modulus of the velocity instead of the streamwise component, U. On the other hand, when dealing with LDA measurements, the pressure term is omitted. Consequently, a combination of these techniques was necessary for getting a correct formulation of Cd.

Thus, by considering two planes, upstream and downstream of the model, normal to the direction of the free-stream, the drag could be expressed from momentum considerations as the sum of several terms, dealing with pressure and velocity contributions:

$$Cd = Cd_{3D} + Cd_p$$

$$Cd = Cd_{2D} + Cd_{vortex} + Cd_p$$

where the reference surface is the total wing area at the model scale. The velocity and pressure contributions are respectively:

$$Cd_{3D} = \frac{1}{\frac{1}{2}S_{ref.}} \int_{wake} \frac{\rho U}{\rho_\infty U_\infty}\left(1 - \frac{U}{U_\infty}\right) dS$$

$$Cd_p = \frac{1}{\frac{1}{2}\gamma M_\infty^2 S_{ref.}} \int_{wake} \left(1 - \frac{P}{P_\infty}\right) dS$$

Cd_{2D} is identical to Cd_{3D}, except that the streamwise velocity component is changed by the velocity modulus. By considering first order's terms, the vortex drag component reads:

$$Cd_{vortex} = \frac{1}{\frac{1}{2}S_{ref.}} \int_{wake} \frac{1}{2}\frac{\rho}{\rho_\infty}\frac{(V^2 + W^2)}{U_\infty^2} dS$$

In order to estimate the drag coefficient of the fuselage alone, those equations have been applied between the upstream plane (stagnation conditions) and the plane located at 120 mm downstream of the model base. It has been also necessary to get rid of the contributions of the horizontal and vertical stabilizers; some difficulties arose because of the strong interaction of the horizontal one and the fuselage.[14] Anyway, one could sort it out by doing exactly the same procedure, whatever configuration was concerned, which justifies the reliability of the following ΔCd values, where ΔCd=$Cd_{\alpha=0°}$ - Cd.

It was found out that:

- increasing the angle of attack of the fuselage from α=0° up to α=2.5° results in a decrease of the total drag coefficient of the fuselage part only: ΔCd=3.5-4.0 10^{-4}.
- the ΔCd induced by the presence of the horizontal stabilizer for a constant value of α is very hard to estimate, since it is almost 0.
- the vorticity contribution in the fuselage drag balance is very dependent upon the aerodynamic configuration, but is somewhat weak. Results are in agreement with preceding observations. Indeed:

Drag coefficient of the fuselage part only			
α(°)	α_e(°)	10^4 Δ Cd	Cd_{vortex}/Cd
0	no	—	1.84%
0	-2	0.3	1.1%
2.5	no	3.4	0.6%
2.5	-2	4.4	0.2%

From the boundary layer calculations performed for the "Fuselage alone" configurations, it has been possible to integrate the friction vector in the surface cartesian frame; that provides the friction drag which can be compared versus the total drag, given from wake surveys. Then, the friction drag is constant when α varies from 0° up to 2.5°, which means that the measured total drag decrease has to be allotted to the pressure drag. The contribution of friction in the drag budget can be estimated to 86% and 90%, for α=0° and 2.5°, respectively. For the configurations, where the fuselage was equipped with the horizontal tail, computation of the friction force was not so easy, because of the existence of areas on the fuselage, where the code stopped.

Conclusions

Thus, those experiments provided a tremendous amount of data, regarding the flow on the rear part of a fuselage. Tests were performed, in the the transonic, pressurized and self-adaptive walls T2-wind tunnel of CERT/DERAT, on a 1/80th scale model of a modern transonic transport aircraft. The model was handled within the wind tunnel test-section through a fin-sting; it was set at two angles of attack, either 0° or 2.5°, whilst the horizontal stabilizer, when present, was set at -2° with respect to the Reference Horizontal Fuselage line. The tests conditions were: a stagnation pressure close to 2 bar, ambient temperature and a free-stream Mach number of 0.82.

The combination of techniques, such as oil-flow visualisations, boundary layer surveys and wake flow measurements, has been a very powerful tool for understanding the physics which develops along the rear part of an upswept fuselage and in the near wake. Indeed, areas of strong cross-flow associated with convergence of wall streamlines were well derived from visualisations. Boundary layer surveys, using 3D LDA system, pointed out the thickening of the boundary layer along the lower symmetry line of the model, whatever aerodynamical configuration was concerned. Furthermore, strong stagnation pressure losses were recorded in the wake of the model, at two diameters downstream of the fuselage base. The use of the LDA system allows to define more precisely, the vortex system associated with these velocity defect pockets, the intensity of the secondary velocity components in some specific areas as well as the exact location of the different vortices.

Those data have helped in the validation of inviscid and viscous codes, developed or used at ONERA; moreover, the limitations of such codes have been indicated. For instance, results of calculations, presented here, show a good agreement between experiments and computations for about 85% of the fuselage length, but not in the downstream part of the fuselage. It is nominally, along the lower symmetry line, where the boundary layer grows rapidly, that the comparison is far from beeing satisfactory.

The choice of turbulence model does not have any influence on the mean velocity profiles but only on the fluctuating ones; this remark is valid under the assumption that the shear stress vector has the same direction as the velocity gradient vector, which might not be true in those areas of strong three-dimensional effects.

The recorded differences between computations and experiments could be attributed to a wrong capture of the streamwise pressure gradient, related to a strong coupling between viscous and inviscid forces, a rather important area where three-dimensionality prevails and, above all, the existence of a pressure gradient in the direction normal to the wall. The boundary layer thickness increases rapidly and must interact with the external flow; one could think that the static pressure might vary within the viscous layer. Moreover, the existence of vortex flow, generated along the rear part of the fuselage, even in the absence of horizontal tail, would suggest to apply Navier-Stokes codes in this rear part of the fuselage. Thus, such boundary layer and wake data, discussed in this paper, would be very helpful, not only for such a validation, but also for future work on turbulence modelling.

It could be noteworthy to mention that further experiments have been performed following on this first set of tests; indeed, a complete wing-body configuration has been studied in order to go closer to flight applications, for the same wind tunnel conditions. Thus, not only the role played by the horizontal tailplane on rear-fuselage flows could be defined but also the action of the wing, for cruise conditions.

Thus, the viscous and inviscid flows in the rear part of the fuselage have been scrutinized for different aerodynamical configurations, following on a couple of experiments carried out in the T2 wind tunnel of CERT/DERAT. The understanding of the observed phenomena could be very helpful, if one wishes to improve the wall flow for such fuselage geometries, by optimizing the shape of the rear part or manipulating the external and wall flows in order to decrease, for instance, the rear-fuselage drag.

Acknowledgements: The experimental as well as numerical researches, reported in this article, have been supported over the last four years, by Airbus Industrie and the Service Technique des Programmes Aéronautiques, that the authors gratefully acknowledge.

References

[1] Séraudie A., Archambaud J-P., Blanchard A., Dor J-B. & Mignosi A.: 3rd ASME-JSME Thermal Engineering Joint Conference on Cryogenic Wind Tunnels.Reno Nevada, March 1991.

[2] Archambaud J-P. & Mignosi A.: Int. Conf. on Adaptive Wall Wind Tunnel Research and Wall Interference Correction, Xian China, June 1991.

[3] Archambaud J-P. & Mignosi A.: Internal Report DERAT N°49/5606.34, April 1992.

[4] Prudhomme S., Séraudie A. & Mignosi A.: 4th Int. Conf. on Laser Anemometry, Cleveland, Août 1991.

[5] Mignosi A., Séraudie A. & Prudhomme S.: 3ème Congrès Francophone de Vélocimétrie laser, Toulouse, Septembre 1992.

[6] Rivoire V. & Eichel P.: Note Technique Aérospatiale 443.528/87, Juillet 1987.

[7] Houdeville R.: 5^{th} Symp. on Numerical and Physical Aspects of Aerodynamic Flows, Long Beach, January 1992.

[8] Houdeville R., Mazin C. & Corjon A.: La Recherche Aérospatiale, 1993-1, January, February 1993.

[9] Malecki P., Cousteix J. & Houdeville R.: 5^{th} Int. Symp. on Refined Flow Modelling and Turbulence Measurements, Paris, September 1993.

[10] Cebeci T. & Smith A.M.O.: Analysis of Turbulent boundary layers. Academic Press, 1974.

[11] Jones W.P. & Launder B.E.: Int. Jour. of Heat and Mass Transfer, Vol. 15, N°2, 1972.

[12] Wolfshtein M.: Int. J. of Heat and Mass Transfer, Vol. 12, 1969.

[13] Norris L.H. & Reynolds W.C.: Report FM-10, Dept. of Mech. Eng., Stanford University, 1975.

[14] Séraudie A., Mignosi A., Dor J.B & Prudhomme S.: AGARD 73rd FDP Meeting and Symposium on Wall Interference Support Interference and Flow field measurements, Brussels, October 1993.